

# Carbon impurity dissolution and migration in bcc Fe-Cr: First-principles calculations

Nils Sandberg,<sup>1,2</sup> Krister O. E. Henriksson,<sup>2</sup> and Jan Wallenius<sup>2</sup>

<sup>1</sup>*Department of Neutron Research, Uppsala University, Uppsala, Sweden*

<sup>2</sup>*Division of Reactor Physics, Royal Institute of Technology, Stockholm, Sweden*

(Received 19 March 2008; published 23 September 2008)

First-principles density-functional theory calculations for C solution enthalpies,  $H^{\text{sol}}$ , and diffusion activation enthalpies,  $H^{\text{diff}}$ , in body-centered-cubic Fe and Cr are presented. The results for C in Fe compare well with experiments, provided that the effect of magnetic disordering is accounted for. Likewise, in Cr, the calculated  $H^{\text{sol}}$  and  $H^{\text{diff}}$  agree well with available experiments. In both materials, the deviation between calculated enthalpies and critically assessed experimental enthalpies are less than 0.05 eV. Further, first-principles calculations for the interaction energies between a solute (e.g., a Cr atom in bcc Fe) and an interstitial C atom are presented. The results are in conflict with those inferred from internal friction (IF) experiments in disordered Fe-Cr-C alloys. A simple model of C relaxation in disordered Fe-Cr is used to compare theoretical and experimental IF curves directly. The results suggest that a more extensive study of the energetic, thermodynamic, and kinetic aspects of C migration in Fe-Cr is needed.

DOI: 10.1103/PhysRevB.78.094110

PACS number(s): 61.72.jj, 64.75.Bc, 66.30.J-, 71.15.Nc

## I. INTRODUCTION

Body-centered-cubic (bcc) (or ferritic) Fe-Cr based steels find applications in high-temperature corrosive environments such as chemical plants and heat exchangers. They have also attracted extensive interest because of their good resistance against neutron irradiation.<sup>1</sup> Thus, both in future energy producing fusion plants and in advanced fission reactors, Fe-Cr based steels are prime candidate materials to be used in structural parts of the reactors that will be subject to extreme neutron irradiation.

Carbon plays a central role in steels, e.g., by stabilizing the face-centered-cubic phase at high temperature, by exerting drag on dislocations and grain boundaries, and by forming carbides.<sup>2</sup> A good understanding of the physics of interstitial C solution and diffusion in Fe, Cr, and in Fe-Cr alloys is of basic importance in order to model the much more complicated metallurgy of Fe-Cr based steels. For instance, parameters such as C solution energies and diffusion activation energies directly influence the kinetics of various phase transformations. In addition, a series of carbides form in the Fe-Cr-C alloys, and the solubility of C depends on which carbides are present in the material.

The Fe-C phase diagram has been studied for more than 100 years.<sup>3</sup> Still, such a basic property as the C solubility in  $\alpha$ -Fe (bcc) is uncertain at low temperatures due to the transition to  $\gamma$ -Fe at 996 K, which makes the determination of a solution activation energy and prefactor difficult. In addition, the transition from ferromagnetic (FM) to paramagnetic ordering in Fe gives a nonlinear contribution to the solubility when viewed in an Arrhenius plot.<sup>4</sup> In contrast, carbon *diffusivity* in the  $\alpha$  phase has been extremely accurately measured (see Ref. 5 for a compilation of experimental data). First-principles density-functional theory (DFT) calculations have provided a detailed atomic level picture of C impurity formation and migration in Fe. Jiang and Carter<sup>6</sup> obtained C solution energies and diffusion activation energies in good agreement with experiments for bcc Fe. However, their analysis did not discuss the effect of magnetism at elevated temperatures.

In the case of bcc Cr, the experimental data on carbon solubility are expected to be more accurate because of the wider temperature range accessible, and because the magnetic transitions occur at lower temperatures compared to Fe.<sup>7</sup> We have found one report<sup>8</sup> giving the solubility of C in Cr. Carbon migration in bcc Cr has been measured by internal friction (IF) (see Ref. 9 and references therein).

The high accuracy of IF methods in measuring migration rates makes it natural to also look at C migration in Fe-Cr alloys. Golovin *et al.*<sup>9</sup> used IF measurements to study the solution and migration of C in disordered Fe-Cr. Their results indicate a nontrivial composition dependence of the effective C migration activation energy in Fe-Cr-C.

The aim of this paper is twofold. First, accurate electronic structure calculations of the solution and diffusion activation energies in bcc Fe and Cr are presented, and critically compared with available experimental data. Second, the interactions between C and host atoms in Fe-Cr alloys are investigated in the framework of the DFT. IF measurements provide an accurate “fingerprint” of the thermodynamics and kinetics of C diffusion in Fe-Cr, therefore also indirectly measuring the carbon-host atom interactions. Our calculated interactions are of similar size, but of opposite sign, to those derived by Golovin *et al.*,<sup>9</sup> based on their IF measurements. Application of a simple model of C relaxation in the alloy, given the interactions derived here, results in IF peaks that are qualitatively different from the experimental ones. Possible reasons for this disagreement are discussed in Sec. IV.

## II. METHOD

### A. First-principles calculations

The current calculations are based on the DFT method as implemented in the VIENNA Ab Initio SIMULATION PACKAGE (VASP).<sup>10</sup> The projector augmented wave (PAW) potentials<sup>11</sup> were used, and a generalized gradient approximation (GGA) (Ref. 12) was chosen as exchange-correlation functional. DFT calculations for defect systems, typically targeting de-

fect energies, require strict settings in order to reach sufficient accuracy. We therefore describe these calculations in more detail below while the specifics of the other calculations, when different, are given later.

A plane-wave cut-off energy of 480 eV was chosen because of the presence of C. The  $k$ -point mesh was  $3 \times 3 \times 3$  for systems of 128 lattice points. When relaxing the atomic positions, we kept the total volume constant (corresponding to the bulk lattice constant) in order to simplify the calculations. For systems with cubic symmetry, the energy lowering upon relaxing the volume can be estimated by use of elastic theory as  $\Delta E = V_0 p^2 / (2B)$ , where  $V_0$  is the volume,  $p$  is the pressure, and  $B$  is the bulk modulus. The octahedral and tetrahedral positions in a bcc crystal have tetragonal symmetry, and the corresponding energy lowering can be expressed as<sup>13</sup>  $\Delta E = V_0 \sigma c^{-1} \sigma / 2$ , where  $\sigma$  is the internal stress tensor and  $c$  is the elastic constant matrix. The internal stress was obtained in the DFT calculations, and the single-crystal elastic constant were taken from Ref. 14. All carbon solution and migration activation energies presented in this paper were corrected in this way. However, because the supercell in these calculations is large (128 lattice points), the corrections are reasonably small (within 0.15 eV).

For an impurity sitting in a substitutional or interstitial site, the defect formation energy is calculated from

$$E_{\text{def}} = E_{\text{def}}^{\text{tot}}(M_n, C) - \frac{n}{N} E_{\text{bulk}}(M_N) - E_{\text{graph}}, \quad (1)$$

where  $E_{\text{def}}^{\text{tot}}(M_n, C)$  denotes a supercell with  $n$  host atoms and one C impurity, and  $E_{\text{bulk}}(M_N)$  is the energy of the defect-free host lattice with  $N$  atoms. For interstitial C structures,  $n=N$ , and for C sitting in a substitutional site,  $n=N-1$ . The energy  $E_{\text{graph}}$  is the C energy per atom in the graphite structure. It is a well-known deficiency of the DFT that it does not describe accurately the binding between the graphite planes, which is due to van der Waals forces. We followed Jiang and Carter,<sup>6</sup> and calculated the C energy by simply constraining the cell parameters for the graphite structure to the experimentally determined ones. The corresponding energy (9.24 eV/atom) agrees reasonably well with a previous plane-wave GGA calculation,<sup>15</sup> in which the relaxed  $c/a$  ratio is however shown to be overestimated.

In Sec. III D, we present results on a study of carbon-solute (C- $s$ ) interaction. It is defined as the energy of a C- $s$  pair at a certain distance, relative to the energies of noninteracting C and solute ( $s$ ),

$$E_{C-s}^f = E_{\text{def}}^{\text{tot}}(M_{N-1}, s, C) - E_{\text{def}}^{\text{tot}}(M_N, C) - E_s^{\text{tot}}(M_{N-1}, s) + E_{\text{bulk}}(M_N). \quad (2)$$

Thus,  $E_{C-s}^f$  is the negative of the binding energy between the carbon and the solute atoms.

With C in the octahedral site being the stable interstitial defect, the solution energy relative to a specific carbide is

$$E^{\text{sol}} = E_{\text{oct}} - E_{\text{carb}}, \quad (3)$$

where the carbide formation energy per carbon atom is

$$E_{\text{carb}} = \frac{1}{n_C} [E_{\text{carb}}^{\text{tot}}(M_n, C_{n_C}) - n E_{\text{bulk}}(M) - n_C E_{\text{graph}}]. \quad (4)$$

Here,  $n_C$  is the number of carbon atoms in the carbide.

### B. Thermodynamic and kinetic relations

At elevated temperature, the solution free energy  $G^{\text{sol}} = H^{\text{sol}} - TS^{\text{sol}}$  will contain the static solution energy,  $E^{\text{sol}}$ , which at ambient pressure can be written as an enthalpy,  $H_{\text{harm}}^{\text{sol}}$ . In addition,  $G^{\text{sol}}$  will contain a number of terms of vibrational, electronic, and magnetic origins,  $G^{\text{sol}} = H_{\text{harm}}^{\text{sol}} - TS_{\text{harm}}^{\text{sol}} + G_{\text{anharm}}^{\text{sol}} + G_{\text{elec}}^{\text{sol}} + G_{\text{magn}}^{\text{sol}}$ . In the present calculations, we assume that the *excess* anharmonic and electronic free energies are small compared to the static free energy. The term  $G_{\text{magn}}^{\text{sol}}$  is important in Fe due to the magnetic transition at the Curie temperature. We have followed the treatment in Ref. 4 in order to take this contribution into account (see Sec. III C 1).

For C at low concentrations,  $G^{\text{sol}}$  is related to the solubility,  $c_C$ , as

$$c_C = 3 \exp(S^{\text{sol}}/k_B - H^{\text{sol}}/k_B T). \quad (5)$$

Here,  $k_B T$  is the Boltzmann constant multiplied by absolute temperature and the factor of three arises because there are three octahedral sites per host atom in the bcc lattice.

The carbon diffusion activation energy in  $\alpha$ -Fe is traditionally assumed to be associated with jumps between octahedral sites via tetrahedral positions (transition states), and it was shown by Jiang and Carter<sup>6</sup> that this picture is consistent with first-principles modeling. In the current paper we have assumed that this applies also for Cr. Then, the activation enthalpy for C diffusion is given by

$$H^{\text{diff}} = H_{\text{tet}} - H_{\text{oct}}, \quad (6)$$

which may again be split into static, vibrational, electronic, and magnetic terms. We will only pay attention to the static enthalpies with the exception of the magnetic contribution to the diffusion activation enthalpy in Fe.

### C. Model of C relaxation

The tetragonal symmetry of the octahedral site in bcc metals gives rise to anelastic effects when interstitial C migrates under an applied tensile stress.<sup>16</sup> This leads to the so-called Snoek effect, which allows for very accurate determination of the migration activation energy via measurements of the internal friction,  $Q^{-1}$ , as a function of the angular frequency,  $\omega$ , of the applied load. In an alloy, we have<sup>9</sup>

$$Q^{-1} = \frac{\delta}{T} \sum_i \left[ \frac{\omega \tau_i}{1 + (\omega \tau_i)^2} \right], \quad (7)$$

where  $\delta$  is the relaxation strength (taken here as equal to unity). The index  $i$  runs over all C atoms, and their respective relaxation times are given by

$$\tau_i = \tau_0 \exp(E_i^{\text{m,eff}}/k_B T), \quad (8)$$

where  $E_i^{\text{m,eff}}$  is an effective migration barrier and  $\tau_0$  is a prefactor for migration jumps taken here as equal for all jumps.

If all C-C, C-Cr, and C-Fe interactions are known, the internal friction can be calculated by means of Monte Carlo simulations. We used a simpler model, in which the relaxation times of noninteracting C atoms in a random Fe-Cr lattice are calculated. Then, only the C-Fe and C-Cr interactions need to be specified. Furthermore, we assumed that the C atoms are thermalized at each temperature. Then, statistical sampling can be achieved by generating random structures with a C atom surrounded by Fe and Cr atoms, and calculate their statistical weight according to the Maxwell-Boltzmann statistics;

$$p_i = \frac{1}{Z} \exp(-E_i/k_B T), \quad (9)$$

where  $Z$  is the partition sum,  $Z = \sum_i p_i$ . For each local configuration  $i$  with energy  $E_i$ , the carbon atom will see four possible jumps directions,  $j$ , with activation energies

$$E_j^{\text{migr}} = E_j^{\text{barrier}} - E_i, \quad (10)$$

where  $E_j^{\text{barrier}}$  is the energy at the barrier dividing the initial and final states of the jump. The expectation time for the escape jump via any of these directions is

$$\tau'_i = \frac{\tau_0}{\sum_{j=1}^4 \exp(-E_j^{\text{migr}}/k_B T)}. \quad (11)$$

Finally, by summing up the contribution from all sites, one finds

$$Q^{-1} = \frac{\delta}{T} \sum_i p_i \left[ \frac{\omega \tau'_i}{1 + (\omega \tau'_i)^2} \right]. \quad (12)$$

### III. RESULTS

#### A. Bulk properties of Fe and Cr

One of the successes with the GGA:s compared to the local-density approximation is the reproduction of the correct ground state for Fe (bcc) and the corresponding magnetic moment. The case of Cr is more difficult because of its peculiar magnetic ground state, which is an incommensurate spin-density wave.<sup>17</sup> However, at low temperatures, it shifts to an antiferromagnetic (AFM) state and, then at 300 K, to a paramagnetic state.<sup>7</sup> The detailed theoretical situation is reviewed in Ref. 17. In the following, we present some calculations for bulk Fe and Cr as a means of checking our calculative methods.

In Fig. 1 we have plotted the calculated total energy and magnetic moment for AF Cr as a function of lattice parameter. It is seen that the equilibrium lattice parameter is less than 1% below the experimental value, and that the equilibrium atomic spin moment is  $0.95\mu_B$ , to be compared to the experimental value  $0.63\mu_B$ . The results in Fig. 1 are essentially in agreement with similar calculations presented in Ref. 17.

Table I summarizes the calculated equilibrium lattice constants, cohesive energies, bulk moduli, and magnetic moments for Fe and Cr, respectively. These quantities were cal-

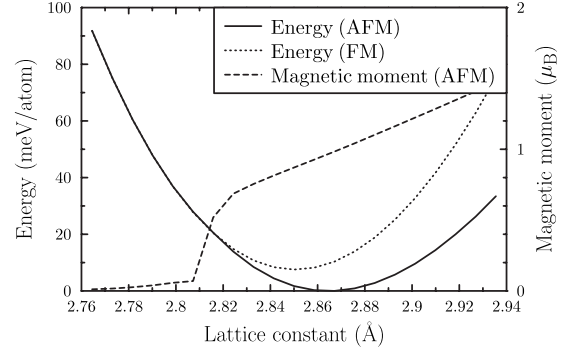


FIG. 1. Total energy and AFM moment as a function of the lattice constant for Cr.

culated from a Birch-Murnaghan fit<sup>18</sup> to the total energy as a function of the lattice parameter. In these bulk calculations, we used a  $20 \times 20 \times 20$   $k$ -point mesh for a conventional unit cell and a cut-off energy of 450 eV. We used both the standard PAW pseudopotentials, which treat the  $3p$  electrons as part of the core, and pseudopotentials, which treat the  $3p$  electrons as valence.

The cohesive energies were calculated by comparing with isolated spin-polarized atoms with the same cut-off energy. The overestimation of  $E_{\text{coh}}$  for Fe is a well-known problem in DFT/GGA.<sup>19</sup> For Cr, the agreement between the calculated and experimental  $E_{\text{coh}}$  is better.

#### B. Carbides

At low temperatures, the stable phases in the case of the Fe-C alloy is  $\alpha$ -Fe and graphite. However, for practical purposes, the metastable  $\text{Fe}_3\text{C}$  cementite structure<sup>20</sup> is usually taken as reference. Pure graphite only forms very slowly at elevated temperatures. The Cr-C low-temperature phases are Cr and  $\text{Cr}_{23}\text{C}_6$  carbide.<sup>21</sup> Thus, the formation enthalpies of cementite and  $\text{Cr}_{23}\text{C}_6$  will determine the reference energies for the solubility of C in Fe and Cr, respectively.

TABLE I. Calculated lattice constants,  $a_0$ , cohesive energies,  $E_{\text{coh}}$ , bulk moduli,  $B$ , and magnetic moments,  $\mu$ , of FM Fe and AFM/FM Cr. Experimental values are given in parenthesis. Results with and without core electrons explicitly included in the DFT calculations are presented.

	$a_0$ (Å)	$E_{\text{coh}}$ (eV/atom)	$B$ (GPa)	$\mu$ ( $\mu_B$ )
pv potentials				
Fe	2.84(2.86 <sup>a</sup> )	5.04(4.28 <sup>b</sup> )	196(173 <sup>c</sup> )	2.20(2.22 <sup>b</sup> )
Cr (AFM)	2.86(2.88 <sup>a</sup> )	4.02(4.10 <sup>b</sup> )	206(190 <sup>d</sup> )	0.95(0.62 <sup>c</sup> )
Cr (FM)	2.85	4.01	258	0.00
standard potentials				
Fe	2.83		188	2.20
Cr (AFM)	2.85		192	0.91

<sup>a</sup>Reference 29.

<sup>b</sup>Reference 30.

<sup>c</sup>Reference 31.

<sup>d</sup>Reference 32.

<sup>e</sup>Reference 17.

TABLE II. Formation enthalpies for carbides in units of electron volts per carbon atom. The reference energies are pure bcc Fe/Cr and graphite structure C at zero pressure.

	Fe <sub>3</sub> C	Fe <sub>23</sub> C <sub>6</sub>	Cr <sub>3</sub> C	Cr <sub>23</sub> C <sub>6</sub>
Calc.	0.18	0.22	-0.33	-0.41
Exp.	0.23 <sup>a</sup>	0.60 <sup>b</sup>	-0.50 <sup>b</sup>	-0.55 <sup>c</sup>

<sup>a</sup>Reference 33.

<sup>b</sup>Reference 22.

<sup>c</sup>Reference 34.

Calculated enthalpies of formation of M<sub>23</sub>C<sub>6</sub> and M<sub>3</sub>C carbides based on Fe and Cr are given in Table II, and compared to values in the literature. In these calculations, we started from the known crystal structure of cementite and Cr<sub>23</sub>C<sub>6</sub>, and relaxed atomic positions and cell shapes. Results for the hypothetical cementite structure Cr<sub>3</sub>C and Fe<sub>23</sub>C<sub>6</sub> are included for reference, and compared with enthalpies derived by Guillermet and Grimvall<sup>22</sup> based on thermodynamic modeling.

### C. Carbon dissolution and diffusion in Fe and Cr

Table III shows calculated defect formation energies, according to Eq. (1), for C sitting in the substitutional, octahedral, and tetrahedral sites in bcc Fe and Cr. As expected, the energetically most stable interstitial site in both bcc Fe and Cr is the octahedral one. Substitutional C in Fe and presumably in Cr sits “off-center” while the present calculations were done with the C in the center of the vacancy. The energy, therefore, does not give information on the vacancy-interstitial binding energy. We include it here because it provides information on the relative binding between C, and Fe and Cr atoms, respectively, in a form that is useful, e.g., in model potential fitting.

Calculated carbon solution enthalpies and diffusion activation enthalpies are given in Table IV. In the following we discuss how these energies are derived from the values in Table III, and how they compare with experiments.

#### 1. Carbon in Fe

In connecting the octahedral defect energy,  $E_{\text{oct}}$ , to the experimentally measured solution energy in Fe,  $H^{\text{sol}}$ , one needs to compensate for two factors. The first is the formation energy of the reference carbide (cementite) and the second is the effect of magnetism. In  $\alpha$ -Fe, C solubilities have been measured in the temperature interval 700–1000 K. This is a region in which  $H^{\text{sol}}$  has a significant temperature depen-

TABLE III. Defect enthalpies for C impurities in bcc Fe and Cr in units of electron volts. The reference states are pure bcc Fe/Cr and graphite structure C at zero pressure.

	Octahedral	Tetrahedral	Substitutional
Fe	0.84	1.64	3.24
Cr (AFM)	1.56	2.66	3.23

TABLE IV. Solution enthalpy,  $H^{\text{sol}}$ , and diffusion activation enthalpy  $H^{\text{diff}}$  for C in bcc Fe and Cr, in units of electron volts. The reference states are Fe<sub>3</sub>C and Cr<sub>23</sub>C<sub>6</sub>, and pure bcc Fe/Cr. Experimental values are given in parenthesis.

	$H^{\text{sol}}$	$H^{\text{diff}}$
Fe	0.81(0.84 <sup>a</sup> )	0.80(0.84 <sup>b</sup> )
Cr (AFM)	1.96(1.98 <sup>c</sup> )	1.10(1.11 <sup>d</sup> )

<sup>a</sup>Reference 4.

<sup>b</sup>Reference 5.

<sup>c</sup>Reference 8.

<sup>d</sup>Reference 9.

dence due to the fact that one is approaching the Curie temperature,  $T_C$ . This magnetic part of the Gibbs energy was divided by Hasebe *et al.*<sup>4</sup> into two parts, stemming from the effect of alloying Fe with C and from the dissolution of cementite. These terms can be estimated based on knowledge of the magnetic Gibbs energy in pure  $\alpha$ -Fe,  $G_{\text{magn}}$ , where we use the expression in Ref. 23, and from knowledge of the change  $\Delta T_C$  in  $T_C$  upon alloying with C. We used  $\Delta T_C = -500$  K.<sup>4</sup> The combined effect of these two factors can be expressed as a magnetic contribution to the C dissolution free energy,  $G_{\text{magn}}^{\text{sol}}$ , relative to the ferromagnetic state. Experimentally, when one reads off an activation energy in an Arrhenius plot,  $G_{\text{magn}}^{\text{sol}}$  will make a contribution  $H_{\text{eff}} \equiv \Delta(G_{\text{magn}}^{\text{sol}}/k_B)/\Delta(1/k_B T)$ . This quantity can be read off in Fig. 2, where  $G_{\text{magn}}^{\text{sol}}$  is plotted in the inset.

In order to compare experimental and theoretical C solubilities, we treated  $S^{\text{sol}}$  as a fitting parameter and fitted to the experimental solubility near the  $\alpha$  to  $\gamma$  transition (see Fig. 3). The resulting  $S^{\text{sol}} = 1.1k_B$  seems reasonable. In Fig. 3 we have plotted the resulting theoretical solubility limit along with experimental data. The theoretical result for the purely FM case, i.e., when  $G_{\text{magn}}^{\text{sol}}$  is ignored, is also shown. An effective high-temperature solution enthalpy is obtained by taking  $H_{\text{eff}} = 0.15$  eV from Fig. 2 as representative for a temperature range between 800 and 1000 K. We then arrive at  $E_{\text{oct}} + E_{\text{carb}} + H_{\text{eff}} = 0.81$  eV, to be compared with the experimental value 0.84 eV.<sup>4</sup>

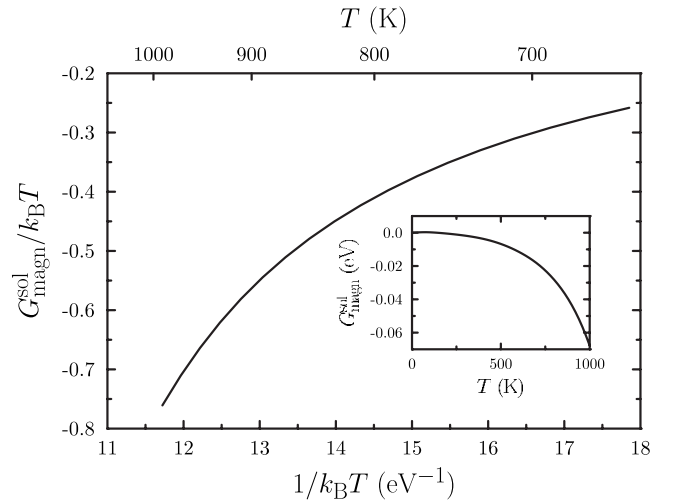


FIG. 2. Magnetic contribution to  $H^{\text{sol}}$  in Fe. The plot is based on the results in Ref. 4. However, we define  $G_{\text{magn}}^{\text{sol}}$  relative to the FM ground state.

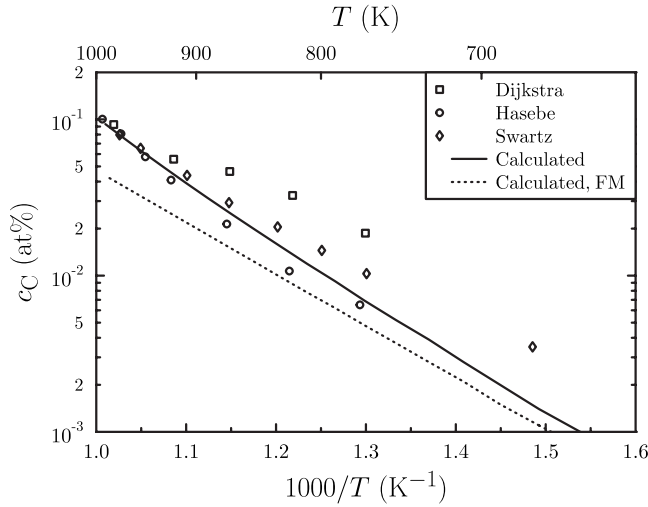


FIG. 3. Solubility limit of C in bcc Fe, calculated according to an Arrhenius form with  $c=3 \exp(S^{\text{sol}}/k_B - H^{\text{sol}}/k_B T)$ , with  $H^{\text{sol}}$  taken from the present calculations, and  $S^{\text{sol}}=1.1k_B$  (solid line). The dotted line shows the solubility when the term  $G_{\text{magn}}^{\text{sol}}$  is ignored, i.e., a hypothetical purely FM solubility limit. Experimental data points from Ref. 25 (diamonds), Ref. 26 (squares) (taken from Ref. 3), and Ref. 4 (circles).

The experimental activation energy for C diffusion in  $\alpha$ -Fe is associated with a transition from the octahedral site to a tetrahedral transition state. Jiang and Carter obtained 0.86 eV, in excellent agreement with the experimental activation energy 0.87 eV given by Wert.<sup>24</sup> Our calculations give  $H^{\text{diff}}=0.80$  eV, i.e., a small underestimation. It should be taken into account that the diffusivity of C in bcc Fe is affected by magnetic disordering, leading to a nonlinear Arrhenius dependence. McLellan and Wasz<sup>5</sup> analyzed this in detail and arrived at  $H^{\text{diff}}=0.84$  eV for the low-temperature (purely ferromagnetic) part of the Arrhenius plot of available diffusion data.

## 2. Carbon in Cr

Table III shows that the Cr interstitial energies are systematically higher compared to Fe, which is in line with experiments that give a very low solubility of C in Cr.<sup>8</sup>

It is, in principle, possible that C sitting in the tetragonal site in Cr does not represent the true saddle point for octahedral-to-octahedral migration. We simply assume that it does, giving  $H^{\text{diff}}=1.10$  eV. This is in excellent agreement with the measurements by Golovin *et al.*,<sup>9</sup> which gave  $H^{\text{diff}}=1.11$  eV.

## D. Carbon-solute binding in Fe/Cr

We now turn to the C solution and migration in Fe-Cr alloys. From the carbide formation energies in Table II, one would expect the C-*s* interaction to be more attractive in the case of Cr compared to Fe. This is also used in the modeling of IF data on C relaxation in Ref. 9. Based on the defect energies in Table III, on the other hand, one would expect the Cr-C interaction in bcc Fe to be strongly repulsive since the defect energy for C in Cr is roughly 1 eV higher than in Fe.

TABLE V. Carbon-solute formation energies (negative binding energies) for C sitting as first, second, and third nearest neighbor to a solute. The interaction with the carbon situated at the maximum distance allowed in the 54 atom supercell is also provided (n-nn). All energies are in units of eV.

Host (solute)	nn	nnn	3rd nn	n-nn
Fe(Cr)	0.28	0.22	0.08	0.05
Cr(Fe)	-0.28			-0.05

In Table V, we summarize the results of a study of the C-*s* interaction in a 54 atom cell. Figure 4 shows the first, second, and third nearest-neighbor octahedral sites from a solute. In these calculations, we used a cut-off energy of 300 eV and  $2 \times 2 \times 2$  *k* points. Thus, the settings were a bit less accurate compared to the 128 lattice-point calculations but, for the present purpose, fully sufficient. In bcc Fe, we find that the Cr-C interaction is repulsive in all C positions around a solute Cr atom. In bcc Cr, the trend is the opposite, i.e., attraction between C and a solute Fe atom.

## E. Internal friction due to C relaxation in Fe-Cr-C alloys

Several experiments show a nontrivial dependence of the effective migration activation energy on the composition in Fe-Cr alloys, as shown in the paper by Golovin *et al.*<sup>9</sup> The effective C migration activation energy increases by 0.4 eV at a Cr concentration of less than 10%, compared to the activation energy in pure Fe. A maximum increase (0.7 eV) is found at 40% Cr, after which the activation energy goes down to the value found in pure Cr. In an attempt to understand how these experimental findings fit with our calculated C-*s* interactions, we carried out a series of simple calculations of the internal friction as a function of temperature and composition, as described in Sec. II C.

In order to model the effect of alloying Fe with Cr, we use a static-lattice model of the host atoms surrounding a C atom, and write the *extra* pair energy of exchanging an Fe atom with a Cr atom as

$$V_{\text{C-Cr}} = V_{\text{C-Cr},0} \exp(-r_{\text{C-Cr}}/\sigma), \quad (13)$$

where  $V_{\text{C-Cr},0}=0.45$  eV and  $\sigma=0.83a_0$  were fitted to the energies in Table V. The barrier energy  $E^{\text{barrier}}$  in Eq. (10) is identified with the energy of one of the four neighboring tetrahedral positions. We use a cutoff between the second and third coordination shell for both the octahedral and tetrahedral sites in the bcc lattice. The calculated  $\Delta H_{\text{Oct}} \equiv H_{\text{Oct,Cr}}$

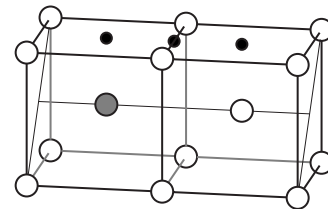


FIG. 4. Octahedral sites in the first, second, and third coordination shells around a substitutional impurity (gray).

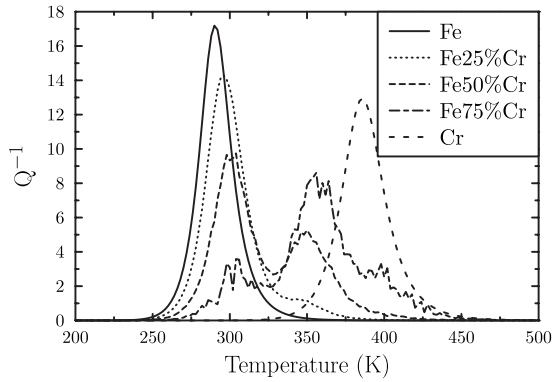


FIG. 5. Calculated internal friction due to carbon relaxation in Fe, Fe-Cr, and Cr.

$-H_{\text{oct,Fe}}=1.26$  eV, and the corresponding  $\Delta H_{\text{tet}} \equiv H_{\text{tet,Cr}} - H_{\text{tet,Fe}}=1.53$  eV, correspond reasonably well with the defect energies in Table III. Thus, Eq. (13) only describes the excess energy of C solution and migration associated with alloying bcc Fe with Cr. However, this is enough to define a model for C relaxation in the alloy. In Fig. 5, we show the calculated internal friction,  $Q^{-1}$ , as a function of temperature and for different Cr compositions varying from zero to one. The calculations were done for  $\omega=1$  Hz, and we used  $\tau_0 = 5.77 \times 10^{-15}$  s.<sup>9</sup> For temperatures in steps of 2 K, we sampled between  $4 \times 10^4$  and  $4 \times 10^5$  random local environments. The calculated  $\Delta H_{\text{oct}}$  is shown in Fig. 6 with  $\Delta H_{\text{oct}}(0)=0$  and  $\Delta H_{\text{oct}}(1)=1.26$  eV.

#### IV. DISCUSSION

The results for C impurity solution and migration in bcc Fe presented in this paper are in good agreement with experimental activation enthalpies. As already mentioned, the accuracy of the experimental migration activation energy data is very good due to the high accuracy of IF measurements. To measure the equilibrium concentration of C in bcc Fe is clearly more difficult. In many of the older measurements, the samples seem not to have been thermalized for long enough times, as discussed in Ref. 3.

Jiang and Carter<sup>6</sup> reported a calculated value of  $H_{\text{migr}}=0.86$  eV, in good agreement with experiments, and  $H_{\text{sol}}=0.74$  eV. The latter value is with reference to graphite and did not take the magnetic contribution into account. This value should rather be compared with our calculated  $H_{\text{oct}}=0.84$  eV, i.e., their value is 0.10 eV lower. In a large supercell calculation, such differences may be due to, e.g., choice of cut-off energy.

The results for dissolved C in AFM bcc Cr agree with several experiments; the activation energy for dissolving C in Cr was calculated to 1.96 eV, to be compared with the experimental value 1.98 eV, and the diffusion activation energy, given by the octahedral-to-tetrahedral transition energy, was calculated to 1.10 eV, compared to 1.11 eV from the experiment. Thus, both results agree very well with experiments.

Thus, our calculated carbon solution and diffusion migration enthalpies agree to within 0.05 eV with experiments.

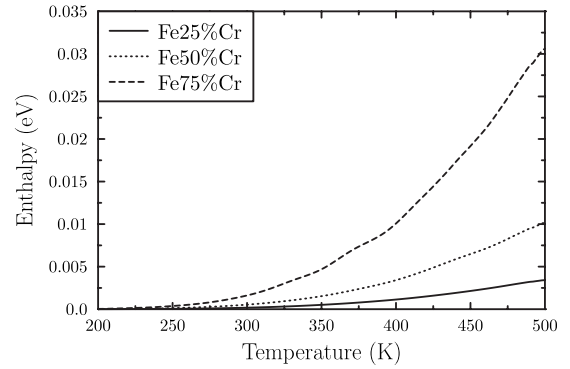


FIG. 6. Calculated C solution enthalpy in a random Fe-Cr alloy, relative to the value in pure Fe.

Such good agreement between calculated and measured defect enthalpies can be contrasted with the case of vacancy assisted diffusion. There, calculations and experiments often disagree by 0.5 eV or more (see, e.g., Ref. 27). An important difference between the formation and migration of interstitial defects, compared with the formation and migration of vacancies, is that the former are not associated with variations in “exposed electronic surface” (see Ref. 28). The good agreement between theory and experiments in the case of C dissolution and migration in bcc Fe and Cr could therefore be expected for interstitial defects in metals in general.

Our calculated internal friction parameters as a function of temperature and for different Fe-Cr compositions show a systematic behavior. There is a gradual shift of the Snoek peak in Fig. 5 from the Fe peak to the Cr peak via a double peak curve. For the 25% Cr alloy, this may be interpreted as follows. The repulsion between C and Cr means that C will essentially stay away from Cr, as realized from Fig. 6. The only process of importance will be the jump into a position with one nearest-neighbor Cr, with activation energy 0.9 eV (with our parameters), and away from that position. The first process will give a peak at around 350, and the second one will have an activation energy close to the one for bulk Fe; it therefore gives no separate peak. For the more concentrated alloys, things should become more complicated, considering that the scatter in both the initial and barrier energies will increase. Clearly, the IF curve, especially for 75% Cr, fluctuates more even though two peaks can still be seen.

In the experiment of Golovin *et al.*,<sup>9</sup> the Snoek peak goes from 310 K in pure Fe to more than 550 K at 35% Cr. This is in quantitative and qualitative disagreement with the present results. There are several possible reasons for this. It seems unlikely that the C-s interaction in Fe and Cr rich Fe-Cr-C alloys would be of opposite sign to the ones calculated here, which is an assumption made by Golovin *et al.* in their modeling of experimental results. The difference is too large to be blamed on uncertainties in the DFT calculations. One possibility is that C-C interactions, which are known to be long ranges due to elastic effects, need to be included as well. The C concentrations used in the experiment by Golovin *et al.* varied between 0.013 and 0.134 at %, which may seem small enough to motivate that C-C interactions are ignored. However, it should be realized that the repulsion

between C and Cr, which underlies the present analysis, strongly limits the number of available sites for C atoms in the alloy at the temperatures in question. Thus, the assumption of negligible C-C interactions, used in the present analysis, may be questionable.

Another assumption underlying the present analysis and the analysis in the paper by Golovin *et al.* is that the Fe-Cr alloy is completely disordered while the C atoms are able to thermally equilibrate perfectly at each temperature. In order to test the validity of this assumption, one would need to perform more detailed kinetic simulations, and more detailed information about the experimental conditions (annealing times, rate of temperature change, etc.) would also be required.

Finally we should mention that magnetic effects, i.e., the loss of ferromagnetism upon alloying Fe with Cr, are expected to influence the C site preference and migration barrier in Fe-Cr, an effect that has not been explicitly included in the current modeling. However, it is again difficult to imagine that this would account for a  $\approx 0.7$  eV increase in  $H^{\text{migr}}$ .

## V. CONCLUSIONS

We have presented first-principles calculations of C impurity formation and diffusion activation energies in bcc Fe and bcc Cr. Good agreement between theory and experiments is obtained for the case of impurities in Fe and Cr and also for carbides with Fe and Cr. The calculated interaction between Cr and C in bcc Fe shows a repulsion of about 0.28 eV in the first shell while the interaction is the opposite (binding) between C and Fe in bcc Cr. Our results are in disagreement with the interpretation of internal friction experiments in Ref. 9, which points to the need of a more exhaustive and realistic study of the energetic, thermodynamic, and kinetic aspects of C migration in Fe-Cr.

## ACKNOWLEDGMENTS

We acknowledge financial support from SKB and EU-ROTRANS domain DEMETRA (EC Contract No. FI6W-CT-2004-516520). A part of the electronic structure calculations presented in this paper was carried out in the CSC's computing environment. CSC is the Finnish IT center for science and is owned by the Ministry of Education.

- 
- <sup>1</sup>D. S. Gelles, *J. Nucl. Mater.* **233-237**, 293 (1996).  
<sup>2</sup>W. Leslie and E. Hornbogen, *Physical Metallurgy of Steels*, 4th ed. (Elsevier, Amsterdam, 1996).  
<sup>3</sup>J. Merlin, P. Merle, S. Garnier, M. Bouzekri, and M. Soler, *Metall. Mater. Trans. A* **35A**, 1655 (2004).  
<sup>4</sup>M. Hasebe, H. Ohtani, and T. Nishizawa, *Metall. Trans. A* **16**, 913 (1985).  
<sup>5</sup>R. B. McLellan and M. L. Wasz, *J. Phys. Chem. Solids* **54**, 583 (1993).  
<sup>6</sup>D. E. Jiang and E. A. Carter, *Phys. Rev. B* **67**, 214103 (2003).  
<sup>7</sup>J. J. M. Franse and R. Gersdorf, *Magnetic Properties of Metals*, Landolt-Börnstein, New Series, Group III, Vol. 19 (Springer-Verlag, Berlin, 1986).  
<sup>8</sup>J. J. Poubeau and J. Bigot, *Acta Metall.* **33**, 1137 (1985).  
<sup>9</sup>I. S. Golovin, M. S. Blanter, and R. Schaller, *Phys. Status Solidi A* **120**, 49 (1997).  
<sup>10</sup>G. Kresse and J. Hafner, *Phys. Rev. B* **47**, 558 (1993); **49**, 14251 (1994); G. Kresse and J. Furthmüller, *ibid.* **54**, 11169 (1996).  
<sup>11</sup>P. E. Blöchl, *Phys. Rev. B* **50**, 17953 (1994); G. Kresse and D. Joubert, *ibid.* **59**, 1758 (1999).  
<sup>12</sup>J. P. Perdew, J. A. Chevary, S. H. Vosko, K. A. Jackson, M. R. Pederson, D. J. Singh, and C. Fiolhais, *Phys. Rev. B* **46**, 6671 (1992); **48**, 4978(E) (1993).  
<sup>13</sup>J. F. Nye, *Physical Properties of Crystals*, 2nd ed. (Oxford University Press, Oxford, 1985).  
<sup>14</sup>G. Grimvall, *Thermophysical Properties of Materials*, revised ed. (Elsevier, Amsterdam, 1999).  
<sup>15</sup>L. Li, S. Reich, and J. Robertson, *Phys. Rev. B* **72**, 184109 (2005).  
<sup>16</sup>J. L. Bocquet, G. Brebec, and Y. Limogue, *Diffusion in Metals and Alloys*, 4th ed. (Elsevier, Amsterdam, 1996).  
<sup>17</sup>S. Cottenier, B. D. Vries, J. Meersschant, and M. Rots, *J. Phys.: Condens. Matter* **14**, 3275 (2002).  
<sup>18</sup>F. Birch, *Phys. Rev.* **71**, 809 (1947).  
<sup>19</sup>E. G. Moroni, W. Wolf, J. Hafner, and R. Podloucky, *Phys. Rev. B* **59**, 12860 (1999).  
<sup>20</sup>F. H. Herbstein and J. Smuts, *Acta Crystallogr.* **17**, 1331 (1964).  
<sup>21</sup>A. L. Bowman, G. P. Arnold, E. K. Storms, and N. G. Nereson, *Acta Crystallogr., Sect. B: Struct. Crystallogr. Cryst. Chem.* **28**, 3102 (1972).  
<sup>22</sup>A. F. Guillermet and G. Grimvall, *J. Phys. Chem. Solids* **53**, 105 (1992).  
<sup>23</sup>M. Hillert and M. Jarl, *CALPHAD: Comput. Coupling Phase Diagrams Thermochem.* **2**, 227 (1978).  
<sup>24</sup>C. A. Wert, *Phys. Rev.* **79**, 601 (1950).  
<sup>25</sup>L. J. Dijkstra, *Trans. AIME* **185**, 252 (1949).  
<sup>26</sup>J. K. Stanley, *Trans. AIME* **185**, 752 (1949).  
<sup>27</sup>N. Sandberg and R. Holmestad, *Phys. Rev. B* **73**, 014108 (2006).  
<sup>28</sup>K. Carling, G. Wahnström, T. R. Mattsson, A. E. Mattsson, N. Sandberg, and G. Grimvall, *Phys. Rev. Lett.* **85**, 3862 (2000).  
<sup>29</sup>W. B. Pearson, *A Handbook of Lattice Spacings and Structures of Metals and Alloys* (Pergamon, Belfast, 1958).  
<sup>30</sup>C. Kittel, *Introduction to Solid State Physics*, 8th ed. (Wiley, New Jersey, 2005).  
<sup>31</sup>J. A. Rayne and B. S. Chandrasekhar, *Phys. Rev.* **122**, 1714 (1961).  
<sup>32</sup>K. W. Katahara, N. Nimalendran, M. H. Manghnani, and E. S. Fisher, *J. Phys. F: Met. Phys.* **9**, 2167 (1979).  
<sup>33</sup>M.-I. Lee and G. Simkovich, *Metall. Trans. A* **19**, 2115 (1988).  
<sup>34</sup>H. Kleykamp, *J. Alloys Compd.* **321**, 138 (2001).